Mechanical properties of tantalum under high pressure

A. Dewaele and P. Loubeyre
Département de Physique Théorique et Appliquée, CEA 91680 Bruyères-le-Châtel, France
(Received 8 March 2005; revised manuscript received 22 August 2005; published 13 October 2005)

We have studied the effect of high pressure, up to 93 GPa, on the yield strength of tantalum single crystals, deformed in a relatively low strain regime (plastic strain smaller than 21%) in a diamond anvil cell. The stress tensor in the sample was calculated by an analysis of its x-ray diffracted signal; the sample strain was determined by an interferrometric method. Even if no dramatic effect of the pressure on the yield stress has been observed, the values of the measured yield strength are higher than expected within the elastic theory of dislocations. This could be due to a coupled effect of pressure and plastic strain.

DOI: 10.1103/PhysRevB.72.134106 PACS number(s): 62.50.+p, 62.20.−x, 61.10.Nz, 07.35.+k

I. INTRODUCTION

The compression of materials under high hydrostatic pressure can significantly affect their mechanical properties. In the 1950s, it was observed that both yield strength and ductility of metals increase with compression, even under relative small pressures ($P<3$ GPa).[1] This increase of strength with pressure is a subject of interest for different fields of physics: the strength of the components of static and dynamic high pressure devices is an important parameter for their design and use; rheological behavior of the Earth's mantle is needed to understand its dynamics.

From a basic materials physics point of view, the macroscopic yield strength, which is the shear stress that allows one to plastically strain a material, is related to different mechanisms of plasticity, from the atomic scale (involving dislocation movements and interactions) to the mesoscopic scale (involving the sliding of grains). Recently, theoretical efforts have been made to better understand the dislocations movements.[2,3] The shear stress required to move an isolated dislocation (the Peierls stress), at ambient pressure[2] and at high pressure,[3] has been evaluated for tantalum. In this last study, it has been obtained that the Peierls stress scales linearly with shear modulus,[3] which confirms the predictions of the elastic theory of dislocations.[4–6] However, the Peierls stress only controls the deformation properties at very low temperature and very low plastic strain ϵ^P. The pressure effect on other mechanisms, which also controls the value of the macroscopic yield strength for $\epsilon^P>0$, such as interactions between dislocations (e.g., cross slip), are still unknown. Measurements of strength under very high pressure, under various plastic strain regimes could help to determine if there actually is a systematic relationship between the yield strength and shear moduli of a material. Compression over a large pressure range is needed to test it: for instance, there is a twofold increase of shear moduli of tantalum between 0 and 100 GPa.

The diamond anvil cell is the only device that allows the generation of static high pressure that reaches and exceeds 100 GPa. There have been numerous studies of the mechanical properties of materials compressed in this device. The yield strength of polycrystalline samples, directly compressed between the diamond anvils, have been deduced from the measurement of the radial pressure gradient in these samples.[7–9] In fact, shear stresses that cause this pressure gradient are only limited by the yield strength of the sample if it is uniformly extruded without slip on the diamond surfaces. However, these kinds of approaches remain qualitative because these assumptions are probably not correct—especially at very high pressure ($P>50$ GPa), when the elastic strain of the diamond anvil prevents plastic flow of the sample.[10] More direct measurements of yield stress have also been performed using x-ray diffraction data and a modeling of the lattice strains in an uniaxially compressed polycrystal.[10–14] For these kinds of studies, diffraction data obtained with the x-ray beam parallel and perpendicular to the load axis of the diamond anvil cell are compared, and the stress tensor in the sample is deduced from this comparison. All these studies were aimed at the determination of the strength of polycrystalline samples. Since samples were directly compressed between the diamond anvils, high plastic strains were achieved at the same time as high pressures were generated: in Ref. 9, the plastic strain was estimated to be between 50 and 100% at 50 GPa. The cumulated effect of pressure and strain has thus been measured in these experiments, exhibiting either strain-hardening (leading to ultrahigh yield strengths) or strain-softening effects.[9,13]

In this work, we have tried to develop an alternative method, which allows us to measure yield strength of materials in a smaller plastic strain domain, using a different sample geometry. To finish, the yield strength of polycrystalline tantalum has already been measured under high pressure.[9] In order to prevent grain boundaries and texture effects, we have chosen to study single crystals. This also avoids any arbitrary isostress or isostrain assumption in the data analysis.[10] Our working material is tantalum, which remains bcc up to approximately 200 GPa,[15] and for which high pressure equations of state have been accurately measured.[16,17] All single crystal elastic constants under high pressure of this metal, needed for the current analysis, have been directly measured to 30 GPa[18,19] and theoretically predicted at higher pressure.[21]

II. EXPERIMENTAL PROCEDURE

A. Principles and conditions of the experiments

Our experiments are aimed at the determination of the yield strength σ_P of a single crystal of tantalum under high

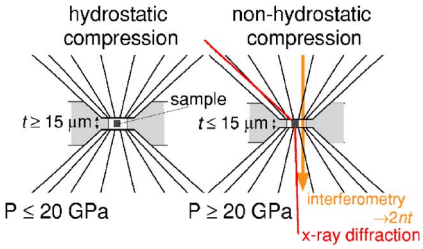

FIG. 1. (Color online) Principles of our mechanics experiment in a diamond anvil cell. At low pressure (left), the sample is embedded in a quasihydrostatic pressure medium. At high pressure, the sample is bridged between the two diamond anvils and is plastically strained if its yield stress is reached. We determine its plastic strain by measuring the thickness t between the anvils by an interferrometric method (see text). We determine the stress in the sample, a single crystal, using x-ray diffraction (see text).

pressure. The sample geometry we have used is schematically represented in Fig. 1. It uses the fact that the space between the diamond anvils decreases with pressure (see Fig. 10 in Ref. 22). At low pressure, the sample was embedded in a quasihydrostatic pressure medium and was elastically strained. At high pressure, the sample was bridged between the two diamond anvils and strains plastically if the nonhydrostatic stress reaches the yield strength. The size of the sample was chosen such that the sample went in contact with the two diamond anvils at a pressure of roughly 20 GPa. It allowed us to achieve very high pressures (90 GPa) with a limited amount of plastic strain of the sample (less than 20%). Since σ_P is expected to vary with plastic strain, this strain has also to be estimated during the experiment. The use of a pressure transmitting medium also allows us to measure the amount of plastic strain in the sample by an interferometric method as explained below. The yield strength σ_P has been calculated using the Tresca yield criterion,[4]

$$\sigma_P \geqslant \sigma_3 - \sigma_1, \tag{1}$$

with σ_3 and σ_1 being, respectively, the maximal and minimal eigenvalues of the stress tensor sustained by a sample. The equality holds if the sample is strained plastically, and the inequality holds if the sample is strained elastically and reversibly. The stress tensor in the sample has been determined by x-ray diffraction, by comparing the distances between various crystallographic planes.

Three experimental runs have been carried out on the ID30 beamline at European Synchrotron Radiation Facility (ESRF) (Grenoble, France) with different mechanical conditions. For runs 1 and 2 (low strain experiment), we increased regularly the membrane pressure (e.g., the force on the diamonds) in order to achieve high pressure and a moderate plastic strain at the same time; for run 3 (high strain experiment), we cycled the membrane pressure in order to achieve high plastic strain at a fixed hydrostatic pressure. For runs 1 and 2, single crystals of tantalum, chosen in a tantalum powder (size 15 μm, 99.9% purity, Goodfellow product) on the basis of their external faceted shape, were loaded in membrane diamond anvil cells[23] with helium or neon as pressure transmitting medium. For run 3, a larger single crystal, synthesized by C. Aracne-Ruddle and D. Farber (Lawrence Livermore National Laboratory, USA), dimensions $25\times75\times75$ μm, oriented (110), has been used. Run 1 has been carried out in the energy dispersive x-ray diffraction (XRD) mode and runs 2 and 3 in the angle dispersive monochromatic XRD mode, at a wavelength of 0.3738 Å (x-ray spot size 10×15 μm). For the energy dispersive experiment, the detector position was fixed at an angle of 6.008° with the x-ray beam (angle calibrated using a copper reference sample). Several peaks diffracted from the single crystal sample have been recorded by rotating the diamond anvil cell around $\mathbf{z_0}$ and the $\mathbf{x}$ axis (see Fig. 3). The energy of the analyzed signal ranged from 15 to 60 keV. For angle-dispersive XRD experiments, the diffracted signal has been recorded on a two-dimensional charge-coupled device (CCD) detector system, located at a distance of 170.350 mm from the sample. The diffraction geometry was determined using a Silicium reference sample. Maximum $2\theta_B$ (θ_B being the Bragg angle) value was 26°. Several peaks diffracted from the single crystal of the sample have been recorded by rotating the diamond anvil cell around $\mathbf{z_0}$ axis (see Fig. 3). Diffraction images were scanned with 100 μm spatial resolution and each single crystal diffracted spot has been individually integrated using the FIT2D software,[24] after refinement of the x-ray beam center.

The experimental conditions of each run are summarized in Table I and photographs of the samples are presented in Fig. 2. For all these experiments, the stress tensor, the plastic strain, and the hydrostatic pressure have been measured at each loading step. The hydrostatic pressure in the chamber was estimated from the luminescence of a small ruby ball and its quasihydrostatic calibration recently refined.[17] The details of stress and strain measurements are explained below.

B. Measurement of stress tensor

For a single crystal, the distance between two atomic planes with Miller index hkl (also called d-spacing) expresses through[25]

TABLE I. Experimental conditions of the three runs.

Run nb.	P_{max} (GPa)	ϵ^P_{max} (%)	XRD Mode	Pressure Medium	Sample Type	Sample Size (μm) (first is the thickness)	Diamond Tip Diameter (μm)
1	65	8	energy dispersive	helium	powder grain	$17\times25\times25$	300
2	90	16	monochromatic	neon	powder grain	$13\times10\times10$	150
3	20	20	monochromatic	neon	polished single crystal	$25\times75\times75$	500

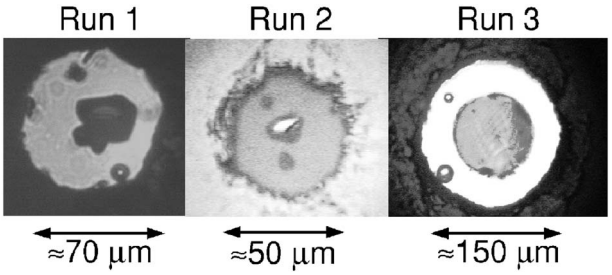

FIG. 2. Photographs of samples for each experimental run at the following pressures: run 1, 15 GPa; run 2, 88 GPa; run 3, 30 GPa. One or two pressure gauges (ruby balls) can be seen in the pressure transmitting medium.

$$\frac{1}{d_{hkl}} = \sqrt{[hkl]\mathbf{G}^{-1}\begin{bmatrix} h \\ k \\ l \end{bmatrix}}, \tag{2}$$

with **G** being the metric matrix related to the elastic strain. In our experiments, the elastic strain can be decomposed in two parts

$$\boldsymbol{\epsilon}^{\mathbf{e}} = \boldsymbol{\epsilon}^{\mathbf{e}}_{\mathbf{H}} + \boldsymbol{\epsilon}^{\mathbf{e}}_{\mathbf{NH}}, \tag{3}$$

the first term represents the hydrostatic part of the elastic strain (which reaches 30% at 100 GPa for tantalum), and the second term the nonhydrostatic part of elastic strain, which remains infinitesimal and satisfies the following condition:

$$\epsilon^{e}_{NH11} + \epsilon^{e}_{NH22} + \epsilon^{e}_{NH33} = 0. \tag{4}$$

In the following analysis, the reference state is the crystal hydrostatically compressed with a lattice parameter a_H. For cubic crystals, the metric matrix is expressed as

$$\mathbf{G} = a_H^2(\mathbf{1} + 2\,\eta^{\mathbf{e}}_{\mathbf{NH}}) \simeq a_H^2(\mathbf{1} + 2\epsilon^{\mathbf{e}}_{\mathbf{NH}}), \tag{5}$$

$\eta^{\mathbf{e}}_{\mathbf{NH}}$ and $\epsilon^{\mathbf{e}}_{\mathbf{NH}}$ being, respectively, the finite Lagrangian strain tensor and the infinitesimal strain tensor, expressed in an orthonormal basis $\mathbf{R}(\mathbf{u},\mathbf{v},\mathbf{w})$ calculated from the crystal lattice by $\mathbf{u}=\mathbf{a}/a_H$, $\mathbf{v}=\mathbf{b}/a_H$, $\mathbf{w}=\mathbf{c}/a_H$. They differ by a quadratic term in strain and are thus close for small strains, which is the case here.

Equations (2), (4), and (5) show that the measurement of six d-spacings d_{hkl} in the same crystal allow the determination of both infinitesimal Lagrangian strain tensor ϵ^e and hydrostatic lattice parameter a_H of this crystal. For the geometry of the diamond anvil cell, the strain parallel to the compression axis $O\mathbf{x}$ of $\mathbf{R}'(\mathbf{x},\mathbf{y},\mathbf{z})$ is expected to be different from the strain perpendicular to $O\mathbf{x}$ (see Fig. 3). Thus, it is important to have x-ray access to atomic planes that have different angles with $O\mathbf{x}$. The large angular aperture of our diamond anvil cells allows us to measure planes with a normal **n** that form an angle from 90° to 55° with $O\mathbf{x}$. In **R**, the stress sustained by the single crystal can be deduced from $\boldsymbol{\epsilon}^{\mathbf{e}}$ using the Hooke's law as follows:

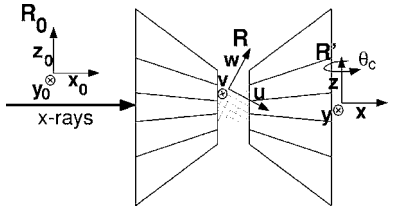

FIG. 3. Definition of the working orthonormal basis used in the calculation of the stress tensor: $\mathbf{R}(\mathbf{u},\mathbf{v},\mathbf{w})$ basis of the sample single crystal; $\mathbf{R}'(\mathbf{x},\mathbf{y},\mathbf{z})$ basis of the diamond anvil cell (**x** parallel to the compression axis); $\mathbf{R_0}(\mathbf{x_0},\mathbf{y_0},\mathbf{z_0})$ basis of the laboratory (x_0 parallel to the incident x-ray beam). $\mathbf{R}'$ can be rotated around $\mathbf{z_0}$ and **x** in energy dispersive XRD experiments, and around $\mathbf{z_0}$ by an angle called θ_C in monochromatic XRD experiments.

$$\sigma = \mathbf{C}\boldsymbol{\epsilon}^{\mathbf{e}}, \tag{6}$$

C being the elastic tensor in the reference state, e.g., under high hydrostatic pressure. For cubic single crystals, all matrix elements of **C** express through C_{11}, C_{12}, and C_{44}, the three independent single crystal elastic constants, in a way detailed in textbooks (see Ref. 25, p. 618). The high pressure values of these parameters are thus needed.

Unfortunately, there is no direct measurement of all single crystal elastic constants of tantalum between 30 and 100 GPa. Accurate ultrasonic measurements of C_{11}, C_{12}, and C_{44} have been carried out up to 0.5 GPa.[18] Stimulated light scattering measurements, leading to C_{11} and C_{44}, have been performed up to 30 GPa.[19] Partial information on elastics constants of tantalum can be also be inferred from its equation of state, measured by x-ray diffraction up to 94 GPa,[17] that allows us to calculate the bulk modulus $K_T = -V(\partial P/\partial V)_T \simeq K_S = (C_{11}+2C_{12})/3$ (the isothermal to adiabatic correction, of the order of 1%,[18] is neglected here). The static elastic constants of tantalum have also been calculated using density functional theory, in the generalized gradient approximation, up to 10 Mbar.[20,21] Indirect measurement of single crystal elastic constants by x-ray diffraction have also been performed,[26] and these data have been reported in Ref. 21. These various data are synthesized on Fig. 4.

To describe the pressure effect on elastic constants C_{ij}, the following form has been proposed,[27] which serves to bound C_{ij} at ultrahigh pressures (the subscript 0 means zero pressure value):

$$C_{ij} = C_{ij0} + \frac{dC_{ij}}{dP}(P=0)P\left(\frac{V}{V_0}\right)^{1/3}. \tag{7}$$

We have used Eq. (7) to extrapolate the most precise data available, provided by ultrasonic measurements,[18] up to 100 GPa. We have validated this method by comparing the extrapolated C_{11}, C_{12}, C_{44}, and K with both experimental and numerical data (see Fig. 4). For single crystal elastic constants, we observe a shift between the parameters obtained by different methods at ambient pressure, but the pressure effect on C_{ij} seems to be correctly modeled by Eq. (7), with the parameters found in Ref. 18. The bulk modulus calculated with this method progressively deviates from the bulk modulus measured by x-rays, the difference reaching 7% at

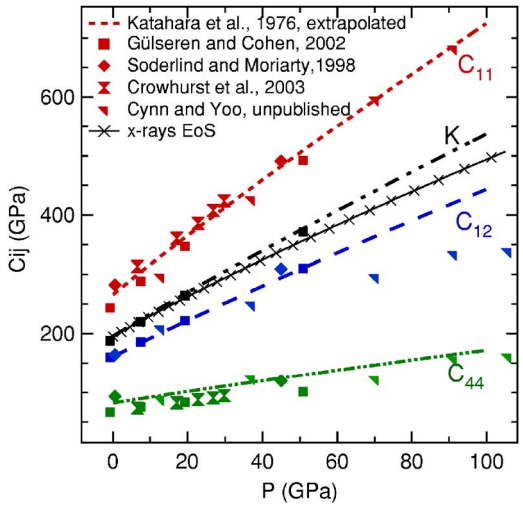

FIG. 4. (Color online) Synthesis of data on elastic constants of tantalum under high hydrostatic pressure found in the literature (Refs. 18, 19, and 17 for experimental studies; Ref. 20 and Ref. 21, for numerical studies). The most accurate data[18] (C_{11}=266 GPa, C_{12}=161 GPa, C_{44}=82 GPa, and dC_{11}/dP=5.1, dC_{12}/dP=3.14, dC_{44}/dP=1.0 at ambient pressure) have been extrapolated using Eq. (7).

100 GPa. In our analysis of x-ray diffraction data, we thus chose to use the values of elastic parameters extrapolated from Ref. 18 using Eq. (7). The expected relative uncertainty highest bound on these parameters is thus 20% at 100 GPa.

C. Measurement of plastic strain

The plastic strain of the sample is deduced from its thickness t. When the sample is in contact with the diamond anvils, its thickness t equals the space between the diamonds (see Fig. 1). The cavity between the diamonds forms a Fabry-Perot cavity, which allows us to perform interferometric diagnostics, if it is filled with a transparent medium.[28] In particular, the interference fringes produced by a parallel white light illuminating the diamond anvil cell can be recorded and analyzed by a spectroscope. The interfringe is expressed as

$$\Delta\sigma = \frac{1}{2nt}, \tag{8}$$

with $\sigma=1/\lambda$ being the wave number of the light and n the refractive index of the transparent pressure transmitting medium (helium or neon). Since the refractive index of these elements has been measured under high pressure,[22] this method allows the measurement of t with an uncertainty of less than 1%. Under the assumption that the crystal is homogeneously strained, the value of t, measured as close as possible to the sample, allows us to estimate the plastic strain in the sample. For that purpose, the interference fringes created in the pressure transmitting medium have been recorded at the sample edge, in order to prevent any bias due to the deformation of the anvils under high pressure.[10] The plastic strain reached in the sample between the beginning of plastic deformation (be), when the sample is bridged between the anvils, and the currents state, can be deduced from the total strain $\boldsymbol{\epsilon}$ and the elastic strain $\boldsymbol{\epsilon}^{\mathbf{e}}$ using

$$\boldsymbol{\epsilon}^{\mathbf{P}} \simeq \boldsymbol{\epsilon} - \boldsymbol{\epsilon}^{\mathbf{e}}. \tag{9}$$

The elastic strain is in major part a hydrostatic strain, as discussed above. We have chosen to express ϵ_H^e using Hencky logarithmic strain: $\boldsymbol{\epsilon}_{\mathbf{H}}^{\mathbf{e}} \simeq \ln[a_H(P)/a_H(P_{be})]\mathbf{I}$. $a_H(P)$ is the lattice parameter of tantalum under hydrostatic compression at the pressure P, the subscript be means beginning of the plastic deformation. The only nonzero component of the total strain $\boldsymbol{\epsilon}$ that is measured in our experiment is ϵ_{11}, in $\mathbf{R}'$, which can also be expressed using logarithmic description of strain (under the assumption that the sample does not rotate): $\epsilon_{11}=\ln(t/t_{be})$. This is a maximum value, based on the approximation that the sample has a cylindrical shape. Using these informations, and the property that $\epsilon_{11}^{\mathbf{P}}+\epsilon_{22}^{\mathbf{P}}+\epsilon_{33}^{\mathbf{P}}=\mathbf{0}$, one can obtain that the plastic stress tensor $\boldsymbol{\epsilon}^{\mathbf{P}}$ has the following form in $\mathbf{R}'$:

$$\boldsymbol{\epsilon}^{\mathbf{P}} = \begin{bmatrix} \epsilon^P & 0 & 0 \\ 0 & -\epsilon^P/2 & 0 \\ 0 & 0 & -\epsilon^P/2 \end{bmatrix} \tag{10}$$

with

$$\epsilon^P = \ln\left(\frac{t(P)a_H(P_{be})}{t(P_{be})a_H(P)}\right), \tag{11}$$

with $a_H(P)$ being the lattice parameter of tantalum under hydrostatic compression at P and the subscript be meaning beginning of plastic strain.

III. RESULTS

A. Rough x-ray data

In this section, we present rough measurements and discuss the analysis of data of the second run, which led to the measurement of the yield stress at the highest pressure (see Table I).

In this run, our visual observations, and the XRD signal collected from the sample, showed that plastic strain had begun at the first step of compression (P=20 GPa). We thus estimated that, with a minor error, this step was associated with the beginning of plastic deformation (P_{be}=20 GPa, t_{be} =16.5 μm). For this step and the following, we have determined the orientation of the single crystal in the diamond anvil cell, using the values of the angle of rotation of the cell θ_C corresponding to the diffraction condition of each peak and the position of the corresponding diffraction peak on the CCD. This allowed us to index the diffraction peaks with Miller notation (hkl) and to determine the rotation matrix from the basis $\mathbf{R}$ to the basis $\mathbf{R}'$. We have followed the ten diffraction peaks marked in Fig. 5. The diffraction information obtained for these peaks at the first deformation step are synthesized in Table II. Plastic strain in the sample caused an important broadening of the rocking curves (in run 1) or x-ray spots (in runs 2 and 3). However, on average, global rotation of the sample during plastic strain has been estimated from x-ray diffraction data and was less than 6° for all

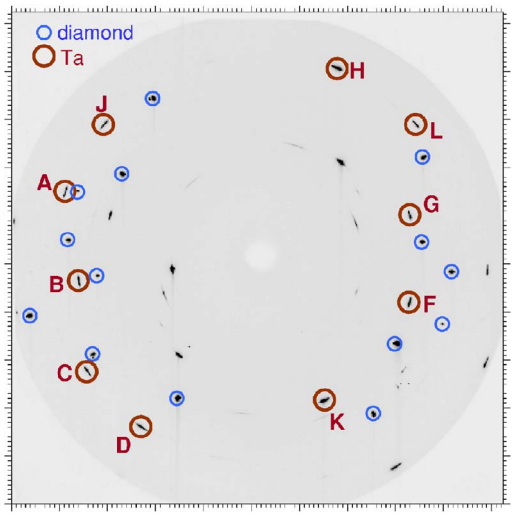

FIG. 5. (Color online) Diffraction data recorded at the first deformation step for run 2 (P=20 GPa). During the x-ray exposure, the diamond anvil cell has been rotated from θ_C=−15° to θ_C=15°. Several spots, surrounded by small circles, are due to x-ray diffraction on the diamond anvils. The other spots are sample signals. The peaks are broadened in an azimuthal angle, indicating that the sample has already been plastically strained. The diffraction peaks used for the determination of the stress tensor have been surrounded by large circles (A to L).

runs. This rotation did not affect our estimate of plastic strain.

The stress tensor determination is based on the comparison between the d-spacings d_{hkl} of these atomic planes. As a consequence, the robustness of the data relies on an accurate determination of the reference of these angles, i.e., the x-ray beam center. For that purpose, the lattice planes with orientations covering the widest solid angle have been studied. Also, the position of the x-ray beam center has been refined using several symmetric diffracted spots for each step of the experiment. We have noted that this position slightly varies with time at the ESRF. Also, in order to reduce uncertainties on the value of d-spacings d_{hkl}, the peaks with the highest values of θ_B have been selected. In runs 1, 2, and 3, d_{hkl} have been measured for (hkl) planes with normal axis having an angle with the compression axis (called θ hereafter) varying between 90° and 69°, 90° and 69°, and 90° and 70°, respectively, and with azimuthal angles homogeneously distributed between 0° and 360° (see Fig. 5). The limited range of θ (90° to 69°) limits the precision of our method. In an ideal case, it should vary between 90° and 0° to precisely measure the elastic strain tensor. This limitation should be overcome with an improved diamond anvil cell design. We have calculated the values of $a_{hkl}=\sqrt{(h^2+k^2+l^2)}\times\lambda/(2\sin\theta_B)$ for each deformation step (see Table II and Fig. 6). In other experiments with the same experimental setup and under quasihydrostatic conditions, the various a_{hkl} obtained from single crystal x-ray diffraction peaks were within $\pm 2\times 10^{-3}$ Å.[16,17] This is not the case here, and the differences increase with increasing strain, as shown in Fig. 6.

B. Stress tensor for runs 1 and 2

Equations (2) and (5) lead to the following equation, which must be verified by each measured d_{hkl}:

$$a_H^2 = d_{hkl}^2[(1-2\epsilon^e_{NH\ 11})h^2 + (1-2\epsilon^e_{NH\ 22})k^2 + (1-2\epsilon^e_{NH\ 33})l^2 + 2\epsilon^e_{NH\ 12}hk + 2\epsilon^e_{NH\ 13}hl + 2\epsilon^e_{NH\ 23}kl]. \quad (12)$$

If 10 diffraction peaks are followed, there are 10 Eq. (12) and one Eq. (4) that must be verified by $\boldsymbol{\epsilon}^{\mathbf{e}}_{\mathbf{NH}}$ (six independent coefficients) and a_H. This overconstrained system can be inverted, and the following tests can be performed to check the validity of the method: (i) all the measured d_{hkl} can be explained by a single elastic strain tensor $\boldsymbol{\epsilon}^{\mathbf{e}}_{\mathbf{NH}}$, within experimental error bars, which is the case here [see Fig. 6(b)]; (ii) the hydrostatic compression parameter a_H at the pressure P

TABLE II. Analysis of the diffraction data recorded at the first deformation step for run 2 (P=20 GPa). The diffraction peaks (A to L) have been indexed with Miller notation (hkl) using the cell rotation angle θ_C, the angle between the diffraction vector and horizontal direction χ, and the Bragg angle θ_B. a_{hkl} is defined by $a_{hkl}=\sqrt{(h^2+k^2+l^2)}\times\lambda/(2\sin\theta_B)$ and would be the same for all diffraction peaks, within $\pm 2\times 10^{-3}$ Å, if the single crystal was hydrostatically compressed.

Peak	(hkl)	θ_C (°)	χ (°)	θ_B (°)	a_{hkl}
A	$(\bar{1}\ 3\ 0)$	−11.5	161	10.6119	3.2094
B	$(\bar{2}\ 2\ 0)$	−6	−172.5	9.4784	3.2101
C	$(\bar{3}\ 1\ 0)$	5	−147	10.6050	3.2115
D	$(\bar{3}\ 0\ 1)$	−10.5	−125	10.6034	3.2119
F	$(1\ \bar{2}\ 1)$	−5	−17.5	8.1923	3.2128
G	$(2\ \bar{1}\ 1)$	5	14.5	8.2020	3.2090
H	(3 1 0)	−8.5	67	10.6323	3.2033
J	$(0\ 3\ \bar{1})$	8	140	10.6088	3.2103
K	$(\bar{1}\ \bar{2}\ 1)$	−11	−64	8.1855	3.2154
L	(3 0 1)	9.5	41	10.6292	3.2042

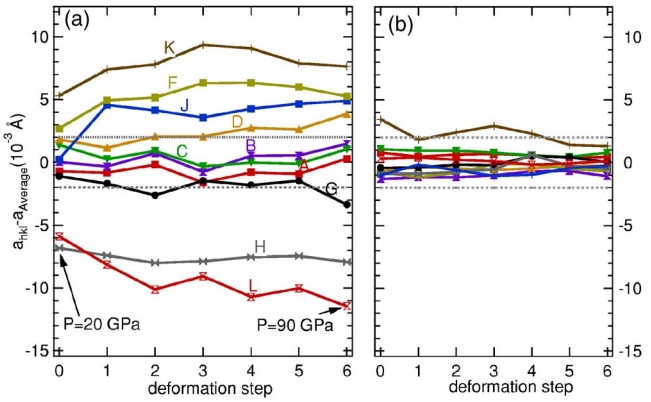

FIG. 6. (Color online) (a) Variations between the values of a_{hkl} obtained from the different diffraction peaks of the same single crystals, labeled A to L (see Table II and Fig. 5). The difference between each a_{hkl} and the average of all a_{hkl} has been plotted. (b) Remaining variations when the elastic strain of the single crystal is taken into account. The difference between each a_{hkl} and the calculated a_{hkl}^{e} of the sample, elastically strained, has been plotted. The dotted lines represent the range of variations of a_{hkl} experimentally measured for a crystal under hydrostatic compression.

obtained in the inversion has to be in good agreement with quasihydrostatic measurements, which is also the case (see Table III); (iii) the stress tensor component is expected to be higher in the direction parallel to the compression axis of the diamond anvil cell than in the other directions, which is also the case, we obtained that the direction of maximum compression is only tilted by 25° from the axis of compression. All these points give us a good confidence in the accuracy of our determination of stress tensor in the case of run 2. The plastic strain presented in Table III has been evaluated, assuming that the first deformation step corresponded to the $P=20$ GPa point and using the measurements of optical thickness $n\times t$ between the diamonds performed at each deformation point and the extrapolation of the refractive index measurements published in Ref. 22.

The same tests have been performed on run 1 measurements, with positive results except for the two last compression points, for which the stress conditions were obviously not homogeneous within the sample. In this run, the pressure in the sample has been slightly corrected because there was radial pressure gradients within this sample due to the uniaxial compression.[9] These gradients have been estimated from our value of $\sigma_3-\sigma_1$ (see Table IV) and Eq. (2) in Ref. 9. It led us to a pressure increase in the sample of 1 GPa at maximum. A similar correction has not been made for run 2, because of the smaller size of the sample. The results are plotted in Table IV. The Tresca stress sustained by the tantalum sample in runs 1 and 2 and are plotted in Fig. 7.

C. Stress tensor for run 3

For run 3, we have been unable to correctly explain the observed d_{hkl} by a single stress tensor from the third deformation step and after. This was probably caused by a too large diameter over thickness ratio of the sample (75 μm in diameter and 25 μm in thickness, see Table I). In fact, if this ratio is larger than 1, inhomogeneous stresses in the sample are expected (see the modeling of mechanical conditions in thin samples in Ref. 8). Thus, this experiment did not lead to conclusive results. The sample geometry, with a diameter much larger than its thickness, is probably not suitable for the current method.

IV. DISCUSSION

Even if obtained in a limited $P-\epsilon^P$ range, and for particular orientations of single crystals toward the compression axis, our measurements of uniaxial stress $\sigma_3-\sigma_1$ (Tables III and IV) allow a qualitative discussion of the effects of P and ϵ^P on the yield strength of tantalum. In fact, the uniaxial stress $\sigma_3-\sigma_1$ equals the Tresca yield strength σ_P [Eq. (1)] if the sample is strained plastically, which occurs without any doubt from step 1 in run 2, and from step 4 in run 1. (We estimate that the absolute error on the measured ϵ^P is of the order of 5%, which includes both error on the measurement of sample thickness and a possible wrong determination of the first step of plastic strain.)

The yield strength σ_P is expected to increase with both hydrostatic pressure and plastic strain, and the following form, which is called the Steinberg-Cochran-Guinan model, that describes this dependency has been often used, at least in the case of polycrystals,[5]

TABLE III. Mechanical conditions of sample strain for run 2. $\sigma_3-\sigma_1$ and a_H are the results of analysis of x-ray diffraction data. a_H^{hydro} is shown for comparison. Estimated error bars on $\sigma_3-\sigma_1$ take into account uncertainties on single crystal elastic constants and on the measured d_{hkl}.

Step	P (GPa)	$n\times t$ (μm)	t (μm)	ϵ^P	a_H Å	a_H^{hydro}[a] Å	$\sigma_3-\sigma_1$ (GPa)
0	20.2	15.90	13.0	0.00	3.2102	3.2073	1.5±1
1	61.0	13.85	10.78	0.14	3.0748	3.0738	3.0±1.5
2	70.8	13.60	10.50	0.16	3.0494	3.0487	3.6±1.5
3	76.0	13.54	10.42	0.17	3.0395	3.0359	3.7±1.5
4	84.0	13.35	10.23	0.18	3.0195	3.0175	5.2±1.5
5	88.3	13.30	10.17	0.18	3.0107	3.0081	4.1±2
6	93.2	12.93	9.86	0.21	2.9994	2.9975	4.4±2

[a]Under hydrostatic compression, using the Vinet equation of state and the parameters of Ref. 17.

TABLE IV. Mechanical conditions of sample strain for run 1. $\sigma_3-\sigma_1$ and a_H are the results of analysis of x-ray diffraction data. a_H^{hydro} is shown for comparison. Estimated error bars on $\sigma_3-\sigma_1$ take into account uncertainties on single crystal elastic constants and on the measured d_{hkl}.

Step	P (GPa)	$n\times t$ (μm)	t (μm)	ϵ^P	a_H Å	a_H^{hydro}[a] Å	$\sigma_3-\sigma_1$ (GPa)
0	11.4	17.82	17.18	0.00	3.2447	3.2446	0.3±0.5
1	15.2	17.79	16.91	0.01	3.2290	3.2275	0.6±0.5
2	20.8	17.71	16.55	0.02	3.2038	3.2039	0.4±0.5
3	25.7	17.76	16.41	0.03	3.1834	3.1846	0.5±0.5
4	31.4	17.38	15.89	0.05	3.1613	3.1626	0.6±1
5	36	17.41	15.80	0.05	3.1449	3.146	1.1±1
6	41	17.28	15.57	0.06	3.1221	3.1293	1.5±1
7	46.6	17.16	15.35	0.06	3.1035	3.1117	1.7±1
8	51.3	16.93	15.06	0.07	3.0907	3.0969	2.6±1
9	57.1	16.94	14.99	0.07	3.0754	3.0812	2.0
10	61.5	16.76	14.77	0.08	3.0555	3.0699	1.6

[a]Under hydrostatic compression, using the Vinet equation of state and the parameters of Ref. 17.

$$\sigma_P(P,\epsilon^P)=\sigma_P(0,0)\frac{\mu(P)}{\mu(P=0)}(1+\beta\epsilon^P)^n. \qquad (13)$$

In the previous equation, it is assumed that the pressure effect on σ_P is proportional to the pressure effect on shear modulus μ, as predicted by elastic theory of dislocations. Within this framework, the strain-hardening factors β and n are assumed to be pressure independent.[6] For a tantalum polycrystal, quasistatically deformed at ambient temperature, the values of β and n vary between, respectively, 17 and 20, and 0.4 and 0.6, with $0.15<\sigma_P(0,0)<0.45$ GPa, depending on the initial crystallographic texture of the sample.[1,30–32] For a high quality single crystal, the values of $\sigma_P(0,0)$ vary between 0.045 and 0.065 GPa, depending on the orientation of the tension axis;[33] these values are expected to be much higher if initial samples have crystallographic defects, which is the case in our study. Fitting the ambient temperature strain-stress curve plotted in Ref. 33 with Eq. (13) leads to values of β and n of 15 and 0.2, but these values are expected to vary with orientation of the single crystal.

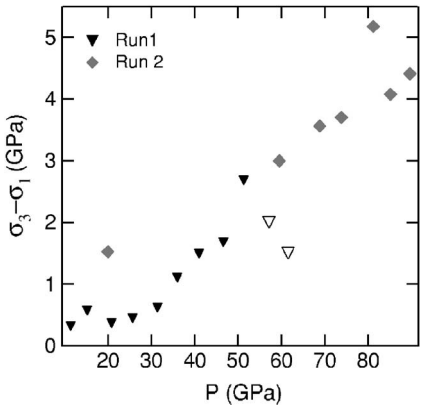

FIG. 7. Tresca stress [see Eq. (1)] sustained by single crystals of tantalum during runs 1 and 2, as a function of the hydrostatic pressure. Empty triangles correspond to inaccurate measurements, because the stress was not homogeneous within the sample.

The values of σ_P under high pressure that we have obtained, as plotted in Fig. 7, are significantly smaller than values found in the literature, for polycrystalline tantalum ($\sigma_P=9.5\pm2.9$ GPa at 44.3 GPa)[9] or for similar metals ($\sigma_P\simeq20$ GPa for tungsten at 200 GPa).[10] Besides the fact that the former experiments have been carried out on polycrystals, instead of single crystals for our experiments, it must be stressed that these experiments have also been carried out at a much larger value of plastic strain (between 50 and 100% at 50 GPa).[9] Unlike in the Ref. 9 study, we did not observe any decrease in σ_P at ultrahigh pressure. Also, the very high values of strain-hardening factors β and n needed to reconcile our data and Ref. 9 data ($\beta\geqslant50$ and $n\geqslant0.5$) suggests that the two types of experiments do not measure the same physical parameters. In our experiments, we did not observe any drastic effect of the sample orientation, runs 1 and 2 leading to comparable values of $\sigma_3-\sigma_1$, despite the different orientation of the single crystal samples in the diamond anvil cell.

Since our experiments have been carried out in a relatively low strain domain ($\epsilon^P\leqslant0.21$), we believe that the current data constitutes the most suitable available experimental constraint on the intrinsic pressure effect on the yield strength of a single crystal at ambient temperature, which is related to both Peierl stress and dislocations interactions. We have tried to isolate an abnormal intrinsic pressure effect on the yield stress by dividing our measured value of yield stress by the shear modulus and by the expected strain-hardening effect, using Eq. (13), and the values of β and n that correspond to average values found in the literature (respectively, 15 and 0.55) for polycrystals, because of the lack of data for single crystals. This normalized yield stress is plotted in Fig. 8 as a function of pressure. It saturates at approximately 40 GPa, to a value that is approximately three times higher than what is predicted by Eq. (13), using literature values of $\sigma_P(0,0)$ for polycrystals. It can be stressed that

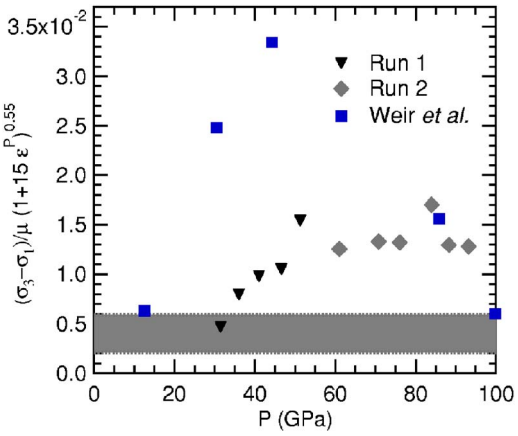

FIG. 8. (Color online) Normalized stress obtained in our experiments (runs 1 and 2) when the sample is plastically strained. Normalization factor corresponds to the expected strain-hardening factor and the expected pressure-hardening factor, i.e., the increase of shear modulus with pressure [see Eq. (13)]. The horizontal lines represent the minimal and maximal value of $\sigma_P(P=0,\epsilon^P=0)/\mu$ at ambient pressure found in the literature. μ has been evaluated using the Voigt-Reuss-Hill average (Ref. 29) and the values of single crystal elastic constants represented on Fig. 4. The error bars on the normalized stress (not plotted) are of the order of 40%. Measurements performed by Weir *et al.* (Ref. 9) are also presented, showing that the literature strain hardening coefficients do not allow us to reconcile the two type of measurements.

from 40 GPa to the maximum pressure reached in our experiments, ϵ^P varies only slightly (by 1% in Run 1 and 7% in Run 2, see Tables IV and III) and that the normalized yield stress in this domain is thus only weakly sensitive to the values of β and n. This saturation of the normalized yield stress thus appears to be a robust result and suggests that pressure effect on the yield strength simply scales with the shear modulus of the material: there is no abnormal pressure-hardening effect. This result is different from the conclusions of previous experimental studies,[9,10] but confirms and generalizes the conclusions of theoretical studies on Peierls stress.[3] However, our measured values of σ^P remain higher than what is expected. This disagreement could be ascribed to a coupled effect of pressure and plastic strain. This effect would be better understood by also carrying out similar experiments in very low plastic strain and very large plastic strain regimes. Unfortunately, only one type of $P-\epsilon^P$ path has been successfully explored in this study (run 3 measurements were not suitable).

V. CONCLUSION

We present here an approach that allows us to measure the mechanical properties under pressure in a diamond anvil cell. It is based on the x-ray diffraction measurement of the stress state of a single crystal and on the interferometric measurement of its plastic strain. It is almost the exact transposition in the diamond anvil cell of the geometry of the mechanical experiments that are usually performed at ambient pressure. The confrontation of single crystal yield strength measurements at very high pressure with theoretical predictions has thus been achieved. The intrinsic effect of pressure on the yield stress is less dramatic than what has been published before.[9,10] In fact, the Steinberg-Cochran-Guinan model is valid with two parameters that fall within their various experimental determination at ambient pressure. A better understanding of coupled pressure and plastic strain effects should be possible by carrying out similar measurements in different P-ϵ^P domains. An improvement of the accuracy of these measurements should be achieved by an increase of the angular x-ray aperture of the diamond anvil cell. Also, the extension of these measurements at high temperature for Earth's mantle materials would have important geophysical implications.

ACKNOWLEDGMENTS

The authors acknowledge the European Synchrotron Radiation Facility for provision of synchrotron radiation facilities on beamline ID30, during beamtime allocated to proposals HS-1361 and HS-1831. We appreciated help of M. Mezouar and A-C. Dhaussy during these experiments. We thank D. Farber and C. Aracne-Ruddle for providing the sample used in Run 3, and M. Berhanu for his help on this project. Discussions with C. Denoual are greatly appreciated.

[1] P. Bridgman, J. Appl. Phys. **24**, 560 (1953).
[2] G. Wang, A. Strachan, T. Cagin, and W. A. Goddard, Phys. Rev. B **67**, 140101(R) (2003).
[3] L. H. Yang, P. Soderlind, and J. A. Moriarty, Mater. Sci. Eng., A **309–310**, 102 (2003).
[4] D. Francois, A. Pineau, and A. Zaoui, *Comportement Mécanique Des Matériaux* (Hermes, Paris, 1995).
[5] D. Steinberg, S. Cochran, and M. Guinan, J. Appl. Phys. **51**, 1498 (1980).
[6] J. Jung, Philos. Mag. A **43**, 1057 (1981).
[7] C-M. Sung, C. Goetze, and H-K. Mao, Rev. Sci. Instrum. **48**, 1386 (1977).
[8] C. Meade and R. Jeanloz, J. Geophys. Res. **93**, 3261 (1988).
[9] S. T. Weir, J. Akella, C. Ruddle, T. Goodwin, and L. Hsiung, Phys. Rev. B **58**, 11258 (1998).
[10] R. J. Hemley, H-K. Mao, G. Shen, J. Badro, P. Gillet, M. Hanfland, and D. Hausermann, Science **276**, 1242 (1997).
[11] G. L. Kinsland and W. A. Basset, J. Appl. Phys. **48**, 978 (1977).
[12] A. K. Singh, J. Appl. Phys. **73**, 4278 (1993).
[13] S. Merkel, H. R. Wenk, J. F. Shu, G. Y. Chen, P. Gillet, H. K. Mao, and R. J. Hemley, J. Geophys. Res. **107**, 2271 (2002).
[14] D. He, S. R. Shieh, and T. S. Duffy, Phys. Rev. B **70**, 184121 (2004).
[15] H. Cynn and C-S. Yoo, Phys. Rev. B **59**, 8526 (1999).
[16] A. Dewaele, P. Loubeyre, and M. Mezouar, Phys. Rev. B **69**, 092106 (2004).

[17] A. Dewaele, P. Loubeyre, and M. Mezouar, Phys. Rev. B **70**, 094112 (2004).
[18] K. Katahara, M. Manghnani, and E. Fisher, J. Appl. Phys. **47**, 434 (1976).
[19] J. C. Crowhurst, J. M. Zaug, E. H. Abramson, J. M. Brown, and D. W. Ahre, High Press. Res. **23**, 373 (2003).
[20] P. Soderlind and J. A. Moriarty, Phys. Rev. B **57**, 10340 (1998).
[21] O. Gülseren and R. E. Cohen, Phys. Rev. B **65**, 064103 (2002).
[22] A. Dewaele, J. Eggert, P. Loubeyre, and R. LeToullec, Phys. Rev. B **67**, 094112 (2003).
[23] R. LeToullec, J-P. Pinceaux, and P. Loubeyre, High Press. Res. **1**, 77 (1988).
[24] A. Hammersley, S. Stevenson, M. Hanfland, A. Fitch, and D. Häusermann, High Press. Res. **14**, 235 (1996).
[25] C. Giacovazzo, *Fundamentals of Crystallography* (Oxford University Press, Oxford, U.K., 1992).
[26] H. Cynn and C-S. Yoo (unpublished).
[27] M. Guinan and D. Steinberg, J. Phys. Chem. Solids **36**, 829 (1975).
[28] J. van Straaten, R. J. Wijngaarden, and I. F. Silvera, Phys. Rev. Lett. **48**, 97 (1982).
[29] J-P. Poirier, *Introduction to the Physics of the Earth's Interior* (Cambridge University Press, Cambridge, U.K., 1991).
[30] K. G. Hoge and A. K. Mukherjee, J. Mater. Sci. **12**, 1666 (1977).
[31] M. Kothari and L. Anand, J. Mech. Phys. Solids **46**, 51 (1998).
[32] S. Nemat-Nasser and R. Kapoor, Int. J. Plast. **17**, 1352 (2001).
[33] T. E. Mitchell and W. Spitzig, Acta Metall. **13**, 1169 (1965).